Carbohydrate Polymers 315 (2023) 120984

Contents lists available at ScienceDirect

Carbohydrate Polymers

journal homepage: www.elsevier.com/locate/carbpol

Fabrication of graded porous structure of hydroxypropyl cellulose hydrogels via temperature-induced phase separation

Alexia Tialiou [a,b], Zahraa H. Athab [c,d], Robert T. Woodward [e], Veronika Biegler [e], Bernhard K. Keppler [a,f], Ahmed F. Halbus [c], Michael R. Reithofer [a,*], Jia Min Chin [g,*]

[a] University of Vienna, Faculty of Chemistry, Institute of Inorganic Chemistry, Währinger Str. 42, 1090 Vienna, Austria
[b] University of Vienna, Vienna Doctoral School in Chemistry (DoSChem), Währinger Str. 42, 1090 Vienna, Austria
[c] University of Babylon, College of Science, Department of Chemistry, Hilla, Iraq
[d] University of Babylon, College of Science, Environmental Research and Studies Center, Hilla, Iraq
[e] University of Vienna, Faculty of Chemistry, Institute of Materials Chemistry and Research, Währinger Str. 42, 1090 Vienna, Austria
[f] University of Vienna and Medical University of Vienna, Research Cluster "Translational Cancer Therapy Research", Währinger Str. 42, 1090 Vienna, Austria
[g] University of Vienna, Faculty of Chemistry, Institute of Inorganic Chemistry—Functional Materials, Währinger Str. 42, 1090 Vienna, Austria

ARTICLE INFO

Keywords:
Gradient porous material
Hydroxypropyl cellulose
HPC
LCST
Thermoresponsive hydrogels
Graded porous hydrogels

ABSTRACT

A novel hydroxypropyl cellulose (gHPC) hydrogel with graded porosity has been fabricated, in which pore size, shape, and mechanical properties vary across the material. The graded porosity was achieved by cross-linking different parts of the hydrogel at temperatures below and above 42 °C, which was found to be the temperature of turbidity onset (lower critical solution temperature, LCST) for the HPC and divinylsulfone cross-linker mixture. Scanning electron microscopy imaging revealed a decreasing pore size along the cross-section of the HPC hydrogel from the top to the bottom layer. HPC hydrogels demonstrate graded mechanical properties whereby the top layer, Zone 1, cross-linked below LCST, can be compressed by about 50% before fracture, whereas the middle and bottom layers (Zone 2 and 3, respectively) cross-linked at 42 °C, can withstand 80% compression before failure. This work demonstrates a straightforward, yet novel, concept of exploiting a graded stimulus to incorporate a graded functionality into porous materials that can withstand mechanical stress and minor elastic deformations.

1. Introduction

In recent years, porous materials gained massive interest in various applications because of their promise in separations, as catalyst supports, and as lightweight materials. Typically, the pores of these materials are uniform throughout the structure. However, functionally graded porous materials consisting of different pore sizes, pore geometry, or porosity across a specific dimension of the materials (Ahmed, Smith, & Zhang, 2011) can be fabricated with either a graded or gradient structure (Miao & Sun, 2009). A graded structure is one whereby there are step-wise changes in the structure, such as that which can be achieved by stacking material components into layers using a variety of methods, while in the gradient structure, the composition of material ingredients changes in a smooth, continuous gradient (Suk, Choi, Kim, Kim, & Kwon, 2003). Many examples of graded/gradient porous materials are found throughout nature, such as bones and teeth which consist of dense shells covering a porous sponge-like structure. Such graded/gradient porosity gives these materials excellent mechanical properties while allowing the transport of chemicals and nutrients throughout the tissue (Wegst, Bai, Saiz, Tomsia, & Ritchie, 2015).

A porosity gradient in functional materials is most commonly used in medical implants to replicate the structures of the parts they are intended to replace, which helps in promoting new tissue growth with the desired mechanical properties (Castillo et al., 2003). Functionally graded materials (FGMs) have also been used as filters for purification and separation applications (Mopoung, Sriprang, & Namahoot, 2014; Souzandeh, Scudiero, Wang, & Zhong, 2017), offering higher separation efficiency than filters with uniform pores (Vida-Simiti, Jumate, Thalmaier, Sechel, & Moldovan, 2012).

Several approaches have been formulated to fabricate structures with graded/gradient porosity, such as sintering of Si/Ti mixtures (Thieme et al., 2001), high-pressure elastomer infiltration into ceramic

* Corresponding authors.
E-mail addresses: michael.reithofer@univie.ac.at (M.R. Reithofer), jiamin.chin@univie.ac.at (J.M. Chin).

https://doi.org/10.1016/j.carbpol.2023.120984
Received 19 September 2022; Received in revised form 14 April 2023; Accepted 2 May 2023
Available online 9 May 2023

preforms (Chabera, Boczkowska, Witek, & Oziębło, 2015), multi-layered tape casting of hydroxyapatite slurries (Werner, Linner-Krčmar, Friess, & Greil, 2002), centrifugation of oil-in-water emulsions (Ahmed et al., 2011), ice-templating of hydroxyapatite (Zuo, Zhang, Jiang, & Zeng, 2011), and even 3D printing of cellulose nanocrystal-based hydrogels (Sultan & Mathew, 2018). Responsive hydrogels with graded porosity have also been prepared. However, these are generally limited to synthetic Poly(N-isopropylacrylamide), PNIPAM-based, hydrogels (Asoh, Matsusaki, Kaneko, & Akashi, 2008; Luo, Wu, Dinh, & Chen, 2015). Alternatively, it is desirable to develop similar responsive hydrogels utilizing natural polymers which are renewable, widely available, non-toxic, and environmentally friendly (Klemm, Heublein, Fink, & Bohn, 2005; Matricardi, Alhaique, & Coviello, 2016). In this context, hydroxypropyl cellulose (HPC), which bears all of these desirable characteristics, is especially interesting.

HPC possesses well-known thermo-responsive properties, whereby its aqueous solutions undergo a phase separation when heated to its lower critical solution temperature (LCST), as the HPC side chains transition from a random coil to a collapsed globular state (Harsh & Gehrke, 1991; Werbowyj & Gray, 1980). The LCST of a polymer refers to the temperature above which the polymer is no longer fully miscible with its solvent, leading to a turbid mixture; below the LCST the components of the polymer mixture are miscible, forming a clear solution. This arises when the polymer/solvent mixing has a negative entropy, which in the case of HPC in water, is due to the high degree of hydrogen bonds formed between HPC and the water molecules during mixing (Taylor, Tomlins, & Sahota, 2017). Such thermo-responsive behavior has been shown to have potential applications in drug delivery (Rahimian, Wen, & Oh, 2015), stimuli-responsive foams (Weißenborn & Braunschweig, 2019) and even smart windows (Nakamura et al., 2019). However, we hypothesize that besides such applications, HPC's thermo-response could also be exploited for the straightforward creation of functionally graded structures by graded temperature exposure of HPC solutions to induce spatially graded phase separation in the HPC solution, which can be fixed during cross-linking into a functionally graded HPC gel. The concept of exploiting temperature induced phase separation (TIPS) to structure hydrogels has been exploited previously, such as for physical gels based on elastin-like polypeptides which demonstrate an arrested phase separation state above their inverse transition temperature (Glassman & Olsen, 2015). Besides elevated temperature, low-temperature induced phase separation can also be exploited, such as for polymer sponges with hard/soft cyclic acetal/polyethylene glycol segments which were photo-polymerized below the solvent crystallization temperature, to generate porosity via solvent crystal templating (K. Wang et al., 2021). However, gels with graded porosity have thus far not been generated via TIPS.

In this work, we, therefore, exploit the temperature-induced phase separation of HPC to create monolithic gels with phase-separation-induced graded porosity. By subjecting different parts of HPC hydrogels to varying temperatures during the cross-linking process and subsequently freeze-drying the gels to generate interconnected pores throughout the material, we report here a simple method of forming HPC hydrogels with graded porosity just by using a temperature gradient rather than complex and tedious layer-by-layer structuring processes. Importantly, this work demonstrates a novel concept of exploiting an inherent stimuli-responsive property of a material by using a graded stimulus to introduce a graded structure in a single step.

2. Experimental part

2.1. Materials for HPC hydrogel synthesis and characterization

Commercially available hydroxypropyl cellulose powder (Sigma-Aldrich) with an average M_w ~ 80,000, M_n ~ 10,000, and 20 mesh particle size, was used as received to fabricate HPC graded porous hydrogel with divinyl sulphone (DVS) 97% (Fisher Scientific, UK) as a chemical cross-linking agent in alkaline media. Sodium hydroxide pellets were purchased from Sigma Aldrich. Purified water was obtained from a Milli-Q reagent water system (Millipore, UK) by passing the water through an Elgastat Prima Reverse Osmosis Unit followed by a Millipore Milli-Q reagent water system consisting of one carbon filter and two ion-exchange filters. This was utilized for all work. Further characterization of the HPC polymer was carried out via gas permeation chromatography (GPC) and differential scanning calorimetry (DSC); $NaNO_3$ and NaN_3 used for GPC were purchased from Sigma Aldrich. Details of the results of the relevant measurements are given in the Supplementary information.

2.2. HPC hydrogel preparation

The graded porosity HPC hydrogel was prepared following a modified version of the Harsh and Gehrke procedure for fabricating uniform HPC hydrogels (Harsh & Gehrke, 1991). 3.5 g of HPC was dissolved in 45.9 mL of 0.01 M NaOH solution at room temperature to make a homogeneous solution. Then, 0.765 g of DVS was added to the mixture, and the reaction was mixed thoroughly for 2 min using a vortex mixer (Vortex-2 Genie). The samples were kept at room temperature for 3 h for initial cross-linking. An addition reaction induced by DVS took place at the hydroxypropyl groups on either the polymer backbone or the substituted groups (Scheme 1). The samples were then partially immersed in a water bath at 42 °C with the help of a styrofoam float, having their upper part above the water level at room temperature (below the LCST) for 6 h. The sample was then removed from the water bath and left at room temperature for 24 h (Kabra, Gehrke, & Spontak, 1998). The selected temperature (42 °C) is slightly lower than the experimentally determined LCST (43.5 °C, Fig. S5), as the DVS presence initiates a pre-crosslinking, already affording a turbid hydrogel at 42 °C.

2.3. Characterization of HPC

Prior to use, commercially available HPC was characterized in detail. Degree of substitution (D.S.) and molar substitution (MS) was determined following literature procedure (Richardson, Andersson, Brinkmalm, & Wittgren, 2003) (see ESI for experimental detail and Fig. S4 for NMR spectra). Lower critical solution temperature (LCST) was obtained through differential scanning calorimetry (DSC) measurements using an aqueous HPC solution (7.46 wt%; see SI for experimental details and Fig. S5 for DSC thermograph). The molecular weight characteristics of the HPC were determined by gel permeation chromatography (GPC) analysis (Fig. S6, Table 1) and showed an M_w and M_n of 108,200 Da and 9400 Da, respectively, consistent with those provided by the supplier (Myrick, Vendra, Le, Sexton, & Krishnan, 2019; Otoni, Lorevice, Moura, & Mattoso, 2018) (see ESI for experimental details and chromatogram). The aforementioned data is summarized in Table 1.

2.4. Scanning electron microscopy (SEM)

Before SEM analysis, freeze-drying was performed; the hydrogels were frozen in the freezer (−21 °C) for 24 h and then immersed in liquid nitrogen before lyophilization. Samples were lyophilized for 3 days using a Beta 2–8 LCSplus – Martin Christ lyophilizer to obtain monolithic FD-HPC hydrogel with graded porosity and interconnected pores.

Scanning electron microscopy (SEM) was performed at the Faculty Center for Nano Structure Research on a Zeiss Supra 55 VP microscope. Samples were carefully prepared to prevent crushing and collapse of the cross-linked/porous network; they were sectioned carefully with a razor blade to create a batch of samples for each individual sample zone. Then, samples were attached to carbon tape at the top of aluminum specimen containers and placed on the specimen holder. They were sputter coated at a Leica EM SCD050 instrument with gold to a thickness of ~5 nm and placed at the specimen stage of the SEM. Measurements were performed at a voltage of 5 kV, magnification range of 40× to 2000×, and with a

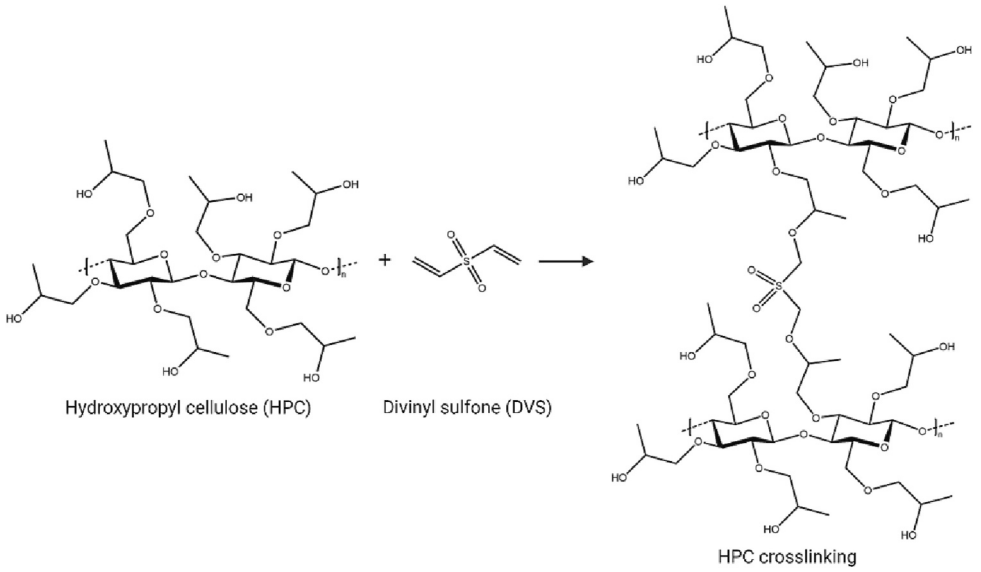

Scheme 1. Chemical structure of HPC and DVS crosslinking to form three-dimensional networks (hydrogel).

Table 1
Summary of the experimental values obtained for the commercial HPC polymer.

D.S.	MS	LCST (°C)	M_w (g mol^{-1})	M_n (g mol^{-1})	M_w/M_n
3	1.41 ± 0.01	43.5	108,200	9400	11.5

Secondary Electrons detector.

2.5. Compression tests

Compression tests were performed using a universal mechanical tester (Model 5969, Instron GmbH) equipped with a 1 kN load cell and a crosshead speed of 1.2 mm·min^{-1}. Cylindrical specimens with a diameter of 25 mm and a height of 15 mm were compressed along the cylindrical axis. All tests were carried out at room temperature at around 23 °C. Their compressional strength was taken as the force applied at the point of structural failure, normalized with the cross-sectional area of the sample. To make direct comparisons between materials, the specimen geometry and size must be accurate. Therefore, the dimensions of each sample are noted to compute stress and strain from load and displacement, respectively. Compressive strain can be calculated using the following equation:

$$\varepsilon_e = \Delta L/L_0 \quad (1)$$

where ε_e is the compressive strain; ΔL is the measured displacement and L_0 is initial specimen length. Compressive stress is calculated by using the equation:

$$\sigma_e = F/A \quad (2)$$

where σ is the compressive stress of the sample (MPa); F is the applied load and A is the initial cross-sectional area of the sample (mm^2). Young's modulus (E) was obtained by linearly fitting the linear elastic region of the stress/strain plots. The Young's modulus, E, characterizes the stiffness of material in units of force per unit area (N·m^{-2}, or Pa). To obtain statistically significant values, six specimens of each sample (non-frozen and frozen) were tested.

2.6. Rheology measurements

Rheology measurements were performed using an HR-2 Discovery Hybrid Rheometer (TA Instruments) in 25 mm diameter aluminum plates with parallel geometry connected to a Peltier plate, and a gap distance of 450 μm. Amplitude sweeps were conducted on crosslinked HPC hydrogel samples to measure their viscoelastic behavior (elastic modulus, G). Sweeps were performed at 10 °C intervals from 25 °C to 55 °C. Within each temperature change, there was an equilibrating of the sample with a soak time of 180 s. The frequency used in amplitude sweeps was 10 rad·s^{-1} and the strain ranged from 1 to 100%. Frequency sweep measurements were conducted within a range of frequency 0.1–100 rad·s^{-1} and strain of 1%. Sample pieces were cut from the crosslinked samples with a sharp razor blade, while they were still supported by the outer shell of the falcon tube. Rheology measurements were repeated three times to obtain statistically significant values and conducted for samples that were subjected to freezing and subsequent thawing as well as samples that were not subjected to freezing. Data analysis was performed with OriginPro, Version 2019 (OriginLab Corporation, Northampton, MA, USA) using 5 points of smoothing.

3. Results and discussion

3.1. Synthesis and morphology of gHPC hydrogels

Falcon tubes (50 mL) containing HPC and DVS were initially allowed to stand at room temperature (22 °C) for 3 h for initial cross-linking and then partially submerged in a water bath (42–43 °C) to prepare graded HPC hydrogels (gHPC) via temperature-induced phase separation (TIPS) as shown in Fig. 1. As shown previously, initial cross-linking of HPC with DVS can take place even at ambient temperature (Harsh & Gehrke, 1991). Cross-linked HPC hydrogel was formed whereby the bottom part of the sample was kept at the LCST, affording an opaque white hydrogel (bottom, Fig. 2A), while the top part was kept at room temperature (22 °C) affording a transparent hydrogel (top, Fig. 2A). The opacity in the bottom part arises due to HPC phase separation and light scattering, while the transparency of the upper part indicates that the HPC remained in a single phase in water.

To verify that all DVS was consumed during the reaction, hydrogels were removed from the Falcon tubes and frozen overnight. The thawed samples were then eluted with 50 mL of milliQ water and left immersed for an additional 30 min in the liquid. The solutions were then concentrated to 15 mL and analyzed by ^{1}H NMR spectroscopy to determine the DVS content. The resulting ^{1}H NMR spectra showed no observable traces of DVS in the eluent (Fig. S2a). In contrast, DVS could only be detected after 2 μL of DVS was manually added to the NMR tube

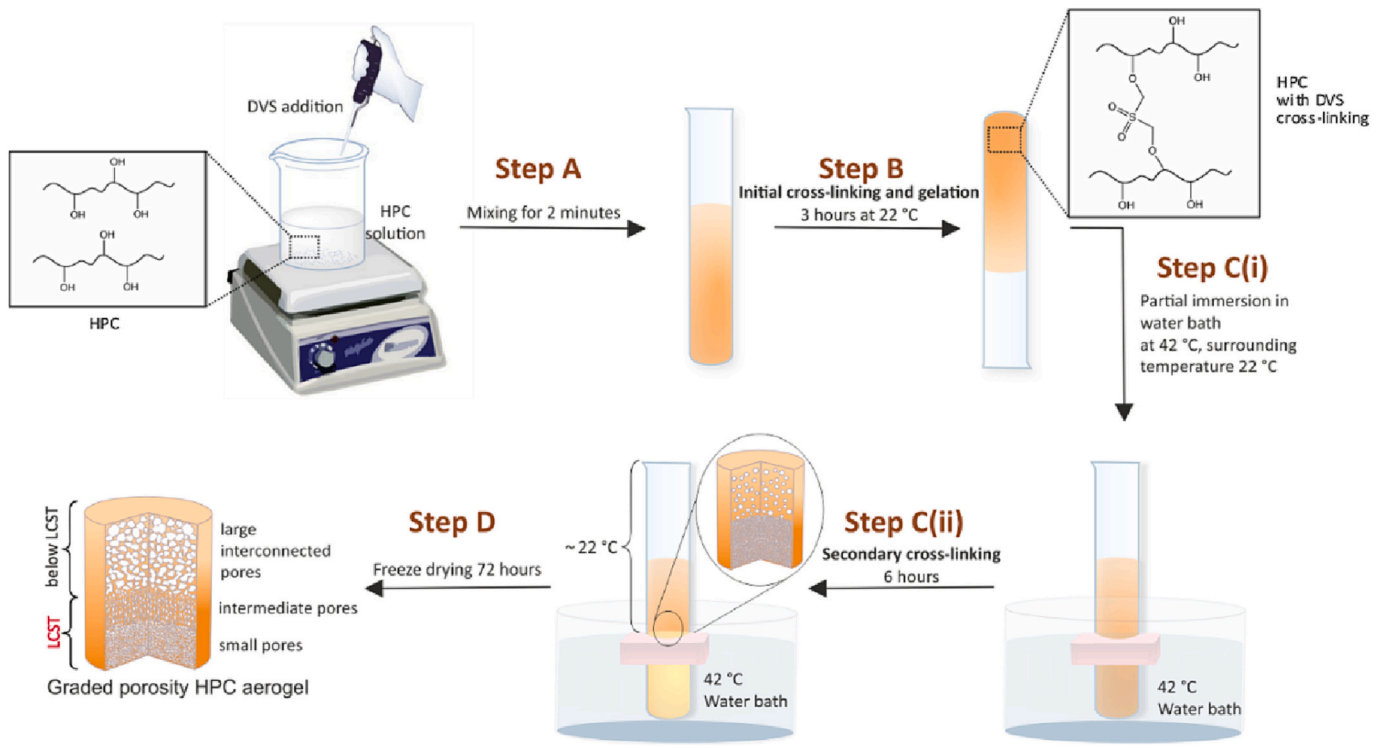

Fig. 1. Illustration of the preparation steps of gradient porous HPC hydrogel (gHPC); (Step A) initial chemical crosslinking at room temperature (22 ± 2 °C) for 3 h; (Step B) settling down at room temperature to initiate gelation; (Step C) partially heating HPC hydrogel with the bottom layer heated at LCST while the top layer is left at room temperature, i.e., below the LCST. This step produces a graded porosity HPC hydrogel; (Step D) Ice templating to introduce pore interconnectivity and freeze drying to produce a permeable graded porosity HPC monolith.

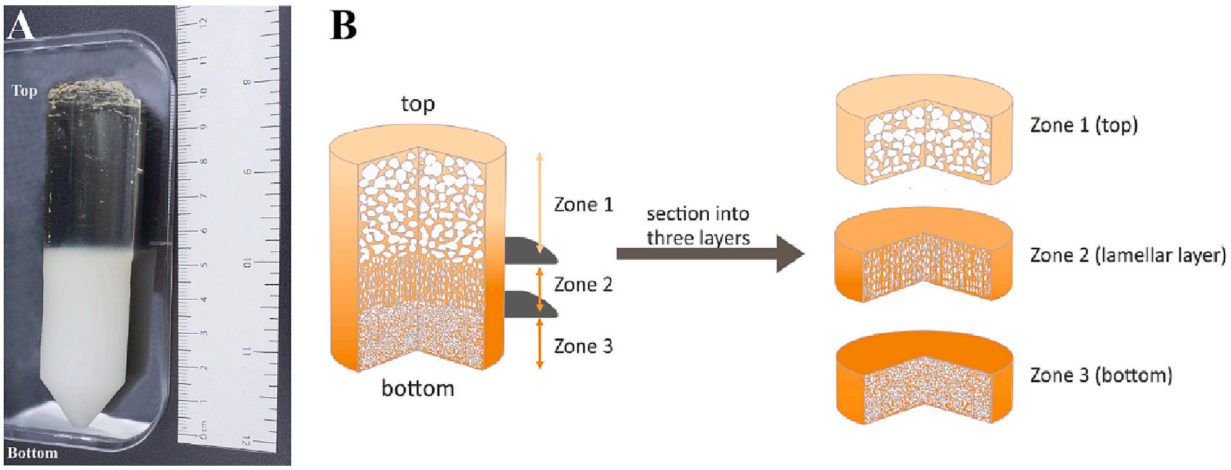

Fig. 2. (A) gHPC hydrogel prepared at a temperature below the LCST (top) and at the LCST (bottom) submerging the sample partially (with insulation foam float to keep the sample upright) in a water bath (42–43 °C). (B) Illustration of freeze-dried graded HPC monolith and its sectioning into Zones 1, 2, and 3, with different pore structures.

(Fig. S2b). Nonetheless, hydrogel samples should be routinely washed if such hydrogels are used as tissue scaffolds or implants.

The gHPC sample was frozen first in the freezer (−21 °C) for 24 h and then submerged in liquid nitrogen to retain the frozen state before loading at the lyophilizer to freeze-dry (FD) for three days. The lamellar ice growth followed by sublimation in the lyophilizer led to large, interconnected pores (below LCST) as well as interconnectivity between pore layers. Before SEM observation, the resulting FD-gHPC monolith was sectioned carefully into three zones (as shown in the schematic of Fig. 2B) and sputter-coated with gold.

Zone 1 (Z1, top layer), cross-linked below the LCST, exhibits a macroporous structure (Fig. 3A) with thick-walled, irregularly shaped pores of approximately 150 to 220 μm in diameter. Below LCST, the sample is hydrated with its pores closed, retaining the water entrapped within its structure. During freezing of this section, lamellar ice growth induces the pore opening/widening via the pushing of HPC to the walls of the structure, making them more rigid and thick. Zone 2 (Z2, middle layer) is formed at approximately the air/water bath interface; this zone shares similar characteristics with Z1. Z2 demonstrates a lamellar structure growing from zone 3 towards Z1; small-interconnected pores of approximately 10 to 60 μm were formed across Z2 (Fig. 3B). Across Z2 a gradual change in porosity of the HPC monolith can be observed

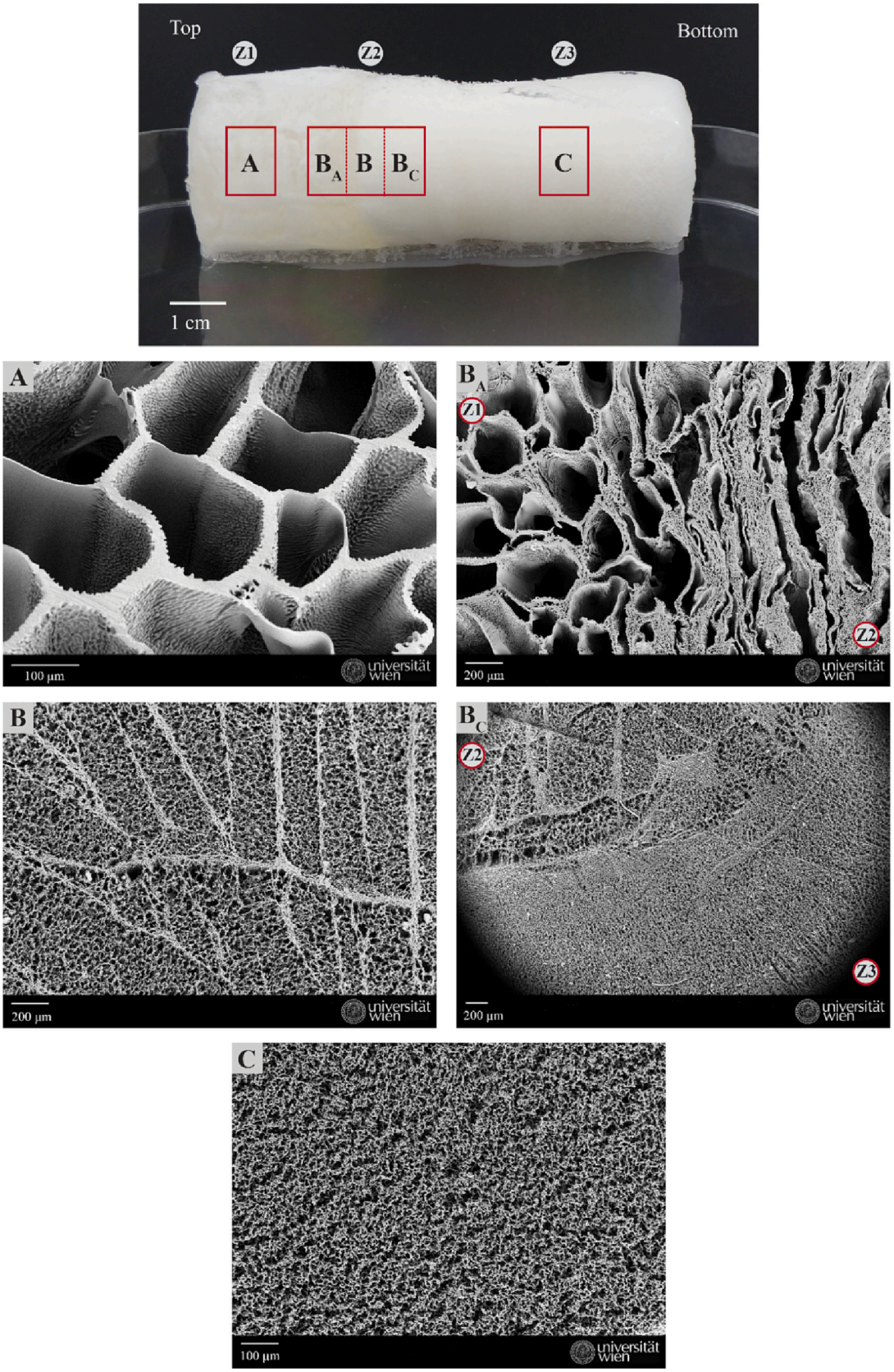

Fig. 3. SEM micrographs depicting the differences between Z1 (A), Z2 (B_A, B, B_C), and Z3 (C) of the freeze-dried gHPC monolith.

(Fig. 3B_A & B_C). Zone 3 (Z3, bottom layer) is formed at 42 °C, a temperature close to the HPC LCST; HPC precipitation and opacity are observed, which are attributed to the breakage of hydrogen bond interactions between HPC and water as well as polymer chain collapse. In Z3, densely packed and even smaller interconnected pores of approximately 3–6 μm can be observed (Fig. 3C). SEM results show a changing pore morphology across the sample, and demonstrate a graded porosity across the HPC monolith from Z1 to Z3. To better characterize the graded structure of the HPC gels, the average pore sizes found in Z1, Z2 and Z3 were measured based on SEM images via ImageJ software. For each zone, 20 pores were randomly selected, whereby the longest (L) and the narrowest (W) part of each pore was measured, calculating the average and standard deviation for each measurement. The average pore size obtained was for Zone 1 L = 330 ± 110; W = 130 ± 50 μm, for Zone 2 is L = 40 ± 20; W = 22 ± 8 μm, and for Zone 3 is L = 12 ± 5; W = 7 ± 2 μm.

In Z2 and Z3, temperature-induced microphase separation occurred after spinodal decomposition of the HPC hydrogel, which was fixed via cross-linking at 42 °C. If cross-linking was carried out significantly below LCST instead, as in Z1, and the sample freeze-dried, the cooling and ice crystal formation lead to phase separation (Annabi et al., 2010) and introduce pore interconnectivity through breaking down of the pore walls, while ice sublimation leaves behind large, interconnected pores.

Separate, non-graded HPC hydrogel samples with the same compositions were prepared; cross-linking was completed at either 42 °C or room temperature. When comparing SEM micrographs of Z1 (FD-gHPC) to non-graded HPC hydrogels prepared at room temperature (FD-HPC_{rt}, Fig. 4) very similar morphologies, with large pores of approximately 150–220 μm in diameter were observed. FD samples of non-graded HPC hydrogels prepared at 42 °C (FD-HPC_{42}) as seen in Fig. 5 also showed a similar pore structure as Z3 (FD-gHPC, Fig. 3C). These observations further confirm that the formation of the graded structure with Z1-Z3 in gHPC arises from the temperature gradient to which the sample is exposed during cross-linking.

3.2. Permeability studies of graded HPC hydrogel

Fluorescein (FL) tracer dye, owing to its low toxicity, high solubility in water, and lack of adsorption behavior in HPC monolith, was used to monitor the diffusion of the aqueous solution through the hydrogel (Einsiedl & Maloszewski, 2005; Plieva, Galaev, Noppe, & Mattiasson, 2008). Previous work by Gehrke and co-workers (Harsh & Gehrke, 1991) showed that as-prepared HPC hydrogels tend to form closed-cell morphologies when the sample was kept below the LCST (decreased cross-linking). It is therefore expected that Z1 of as-prepared gHPC hydrogels would possess a closed-pore morphology and would not exhibit water permeability. To confirm this, gHPC hydrogels were prepared as columns directly in plastic syringes (20 mL) for tracer tests, to evaluate fluid transport behavior in the hydrogels. A tracer test was performed at room temperature (22 ± 1 °C) on two gHPC hydrogel samples to evaluate permeability. One of the samples was subjected to freezing at −21 °C for 1 day and subsequent thawing before the tracer test. As shown in the left column in Fig. 6A, the FL dye solution does not permeate the top layer of the as-prepared gHPC hydrogel, supporting the hypothesis of closed pores in this region. However, after overnight freezing and thawing, the gHPC hydrogel column showed fast spreading

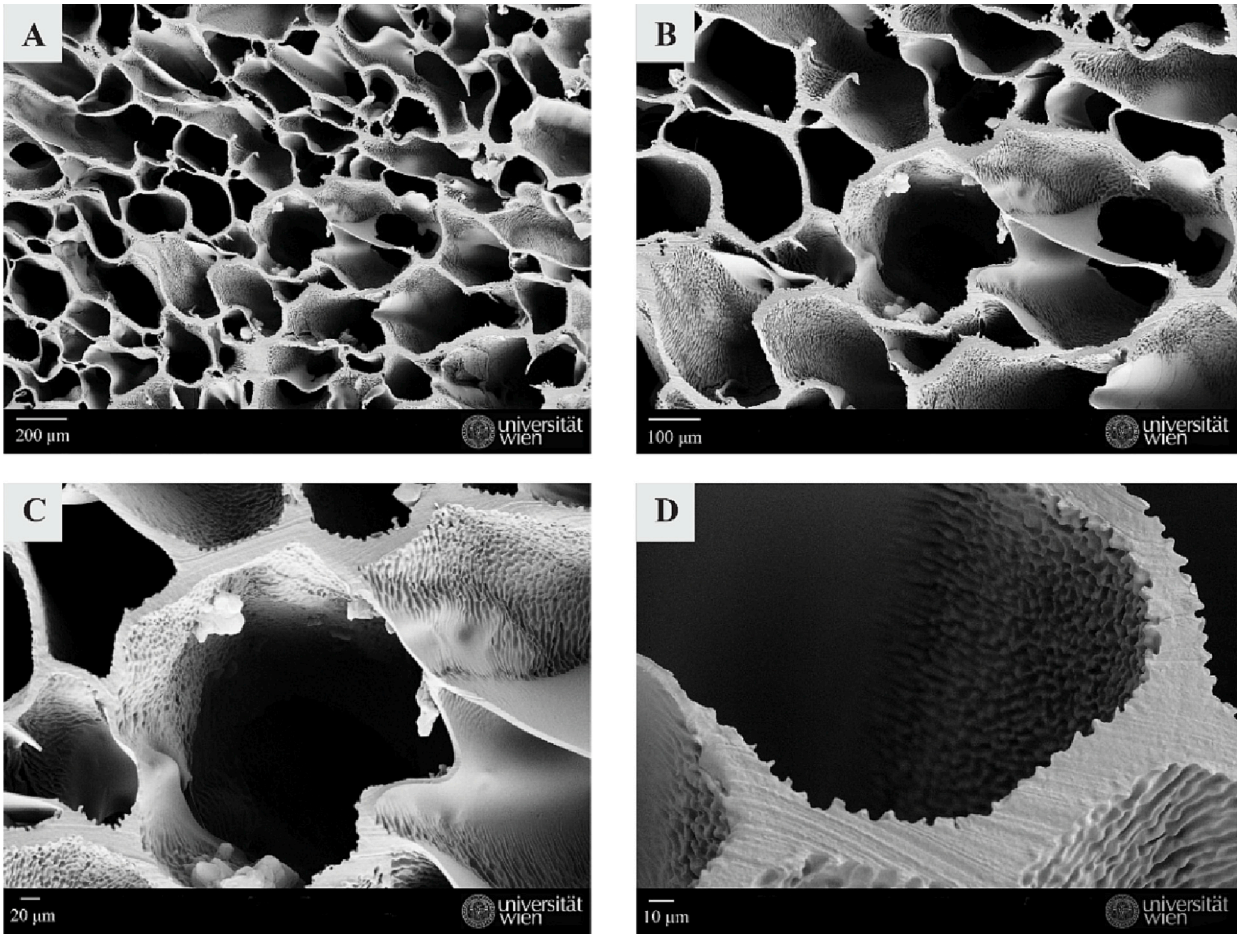

Fig. 4. SEM micrographs of freeze-dried HPC hydrogels prepared at room temperature (22 ± 3 °C) at different magnifications. Scale bars represent (A) 200 μm (B) 100 μm (C) 20 μm (D) 10 μm.

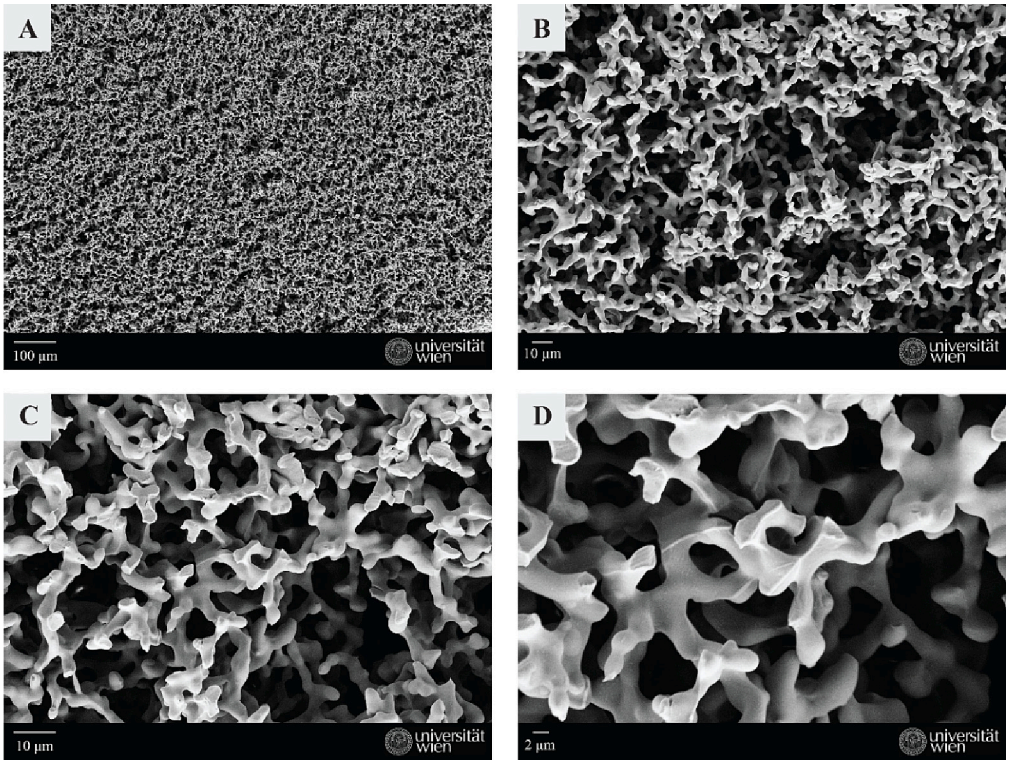

Fig. 5. SEM micrographs of freeze-dried HPC hydrogels prepared at 42–43 °C at different scales and magnifications (A) 100 μm (B) 10 μm (C) 10 μm and (D) 2 μm.

of the fluorescein dye throughout the monolith as shown in the right column in Fig. 6B, indicating pore interconnectivity in Z1, introduced via the freezing process (Plieva et al., 2008; C. Wang et al., 2018). During freezing, the nucleated ice crystals grow and act as macropore templates (Grenier et al., 2019). The melting of these ice crystals above the freezing temperature gives rise to interconnected macroporous networks (Gun'Ko, Savina, & Mikhalovsky, 2013).

3.3. Mechanical properties of gradient HPC hydrogel

3.3.1. Rheology

Characterization of the gHPC hydrogels was done by oscillatory rheology to monitor the viscoelastic behavior. Rheology measurements were performed by keeping either the frequency at a constant value of 10 rad·s^{-1} or strain at 1% and monitoring the changes upon temperature changes for Z1, Z2, and Z3 of gHPC hydrogels. All measurements were conducted for samples without and with a freeze-thaw cycle (referred to below as non-frozen = NF, and frozen = F samples, respectively). Plots of the storage (G′) and loss (G″) moduli of the hydrogels against angular frequency and strain can be seen in Fig. 7, and Figs. S11, S12, and S13 of the Supplementary material.

As shown in Fig. 7, the storage modulus, G′, increases with frequency; the shear rate also increases with the increment of frequency meaning that there is a simultaneous increase in the energy input applied to the polymer chains. During frequency sweeps, the G′ of Z1, Z2 and Z3 measured at different temperatures is consistently higher than the loss modulus, G″, in both NF and F samples. This indicates that the material shows a gel-like elastic behavior rather than a liquid-like viscous one, as expected due to their DVS-crosslinked network. In Z3, different G′ values are observed at different temperatures. Z3NF at 25 °C possesses a higher G′ than Z3F, demonstrating a better elastic character. Freezing of Z3 may have led to the perforation of some pore walls due to ice crystal formation, leading to a weaker material. However, at 45 °C (above LCST), G′ of Z3NF is significantly decreased compared to that at 25 °C, suggesting that phase changes led to pore wall weakening. In contrast, G′ of Z3F increased at 45 °C, leading to a crossover at low angular frequency (17 rad·s^{-1}), whereby G′ of Z3F is higher than that of Z3NF.

G′ and G″ moduli of Z1NF are significantly higher at temperatures 35, 45, and 55 °C compared to 25 °C (Table 1, Fig. S12); the entrapped water in the closed pores of Z1 increases the G′ and G″. At all measured temperatures, Z1, and Z2 samples show an increase in G′ after freezing, which may be due to the thickening of pore walls during ice-crystal formation, whereby HPC chains extending into the pore chambers are pushed out towards the pore walls, making them thicker and stiffer, despite ice growth creating openings between initially closed pores. The highest G′ values among NF and F samples are demonstrated at a temperature below the LCST for Z3NF (0.23 MPa) and Z2F (0.12 MPa), respectively (Table 2). Interestingly, Z1NF, Z2NF, and Z3NF show a progressively increasing G′ (0.005, 0.02, 0.16 MPa respectively) when measured at 25 °C, indicating that increasing the crosslinking temperature to the LCST or above enhances the mechanical properties of the gel, which may arise from an increased degree of cross-linking from Z1 to Z3. The results also conclusively support the presence of an elastic modulus gradient lengthwise along the gel monolith.

Amplitude sweeps of different zones show the difference in rheological behavior of the material within 1–100% applied strain (Fig. S11). Amplitude sweep measurements show that Z3NF has a higher storage modulus and hence better elastic behavior than Z3F. In contrast, Z2F demonstrates better elastic behavior than Z2NF. Comparing the non-frozen samples, Z1NF has the lowest storage modulus, followed by Z2NF and then Z3NF, indicating that the gel monolith possesses a vertical elastic gradient. Additionally, amplitude sweeps of Z1F, Z2NF/F, and Z3NF/F demonstrate a crossover of G′ and G″ moduli with G′ < G″ highlighting a change from an elastic-like behavior to a more viscous liquid-like one at higher strain (Supplementary, Table S1, S2). In Z1F and Z2F, crossovers with similar strain% are observed at 25 °C (2–9%), 35 °C (15–18%), and 45 °C (39–40%).

In conclusion, the freezing contributes to the formation of larger interconnected pores; the pore walls become considerably thicker

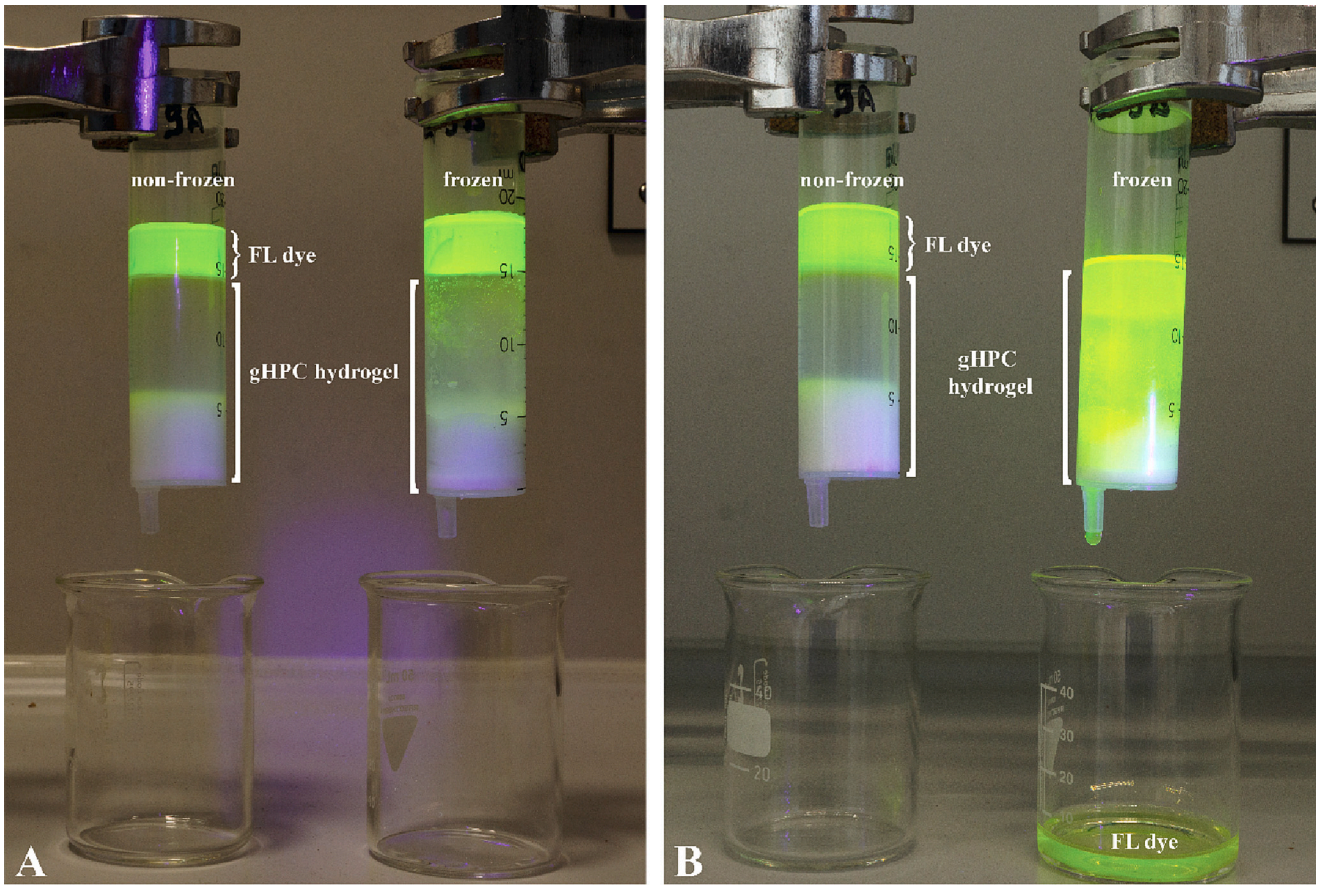

Fig. 6. Evaluation of pore connectivity of the gHPC hydrogel samples without freezing (referred to as non-frozen) and with freezing (−21 °C) and subsequent thawing (referred to as frozen) (A) at t = 0 s and (B) at t ≈ 2 h via a dye tracer test using fluorescein under 365 nm illumination. The tracer solution is only able to flow through the sample with freezing treatment.

leading to an increase of G′ and prevailing elastic properties. The aforementioned increase is reported in Table 1 for Z1F and Z3F. In general, below LCST (Z1, Z2) samples demonstrate better elastic behavior after freezing, whereas above LCST (Z3) non-frozen samples demonstrate similar behavior.

3.3.2. *Compression tests*

The mechanical properties of the graded HPC hydrogel were further investigated through uniaxial compression testing on sectioned layers of the NF and F hydrogel. Fig. 8A shows the compressive stress-strain curves of Z1, Z2, and Z3 of the hydrogels, both before and after freezing.

It can be seen from the curves that Z2 and Z3 of the graded hydrogel can be compressed to approximately 20% of the original cylinder height without fracture. The compressive stress in Z2 and Z3 gradually increased with increasing strain until the compressive strain was approximately 60%; above this point, it suddenly increased and showed typical "J" shaped curves, indicating their high compressive strength. In comparison, Z1NF of the gHPC hydrogel shows fracture at a low deformation of about 53%, while the same layer after freezing (Z1F) exhibited around 49% compression strain without mechanical destruction or permanent deformation.

The compressive modulus was obtained as the slope by linearly fitting the stress-strain curve at the initial stage with a strain between 5 and 15%. Fig. 8B shows the compressive modulus of each zone calculated from the strain-stress curve. Z1NF and Z1F demonstrate statistically significant difference. Z1NF gives a compressive modulus of ~0.0169 MPa in compression, which decreases to 0.011 MPa after freezing, which is attributed to the breakage of pore walls due to ice crystal growth during freezing. This is in line with the observations by Bencheri and coworkers whereby freezing reduced the Young's modulus of the hydrogel materials (Bencherif et al., 2012). The difference of Young's modulus of Z2 and Z3 is not statistically significant. However, there is an indication of reduction of Young's modulus for Z2NF, demonstrating a compressive modulus of 0.028 MPa, which decreases to 0.026 MPa after freezing. Z3NF though demonstrates a compressive modulus of 0.022 MPa, which increases to 0.027 MPa after freezing. Z3NF has good mechanical properties due to its elastic porous structure; after freezing its stiffness increases, contributing to better mechanical properties. gHPC samples exhibit graded mechanical properties. The entrapped water in Z1 and Z2 impacts the hydrogel's fragility; after freezing the opening of the pores partially damages the material which is unable to endure the same amount of mechanical stress compared to its NF form. Z3, which already has an open porous structure, improves its stiffness after freezing, affording better mechanical properties similar to ones of Z2NF.

It is worth mentioning that trends observed by rheology might not be confirmed by compression test. This discrepancy between these two methods may arise from the inherent anisotropic structure of the investigated hydrogels, caused by the direction of heat transfer during the cross-linking process, as well as the different direction of applied forces in each characterization method. In the measurement of G′, an oscillating shear force is applied to the samples, forcing the vertical pore walls to twist. In the compression test, however, the pore walls buckle under compressive stress. As the samples have anisotropic structures, with non-symmetric, non-spherical pores, a trend in G′ does not equate to the same trend in compressive modulus. Thus, the inherent structural anisotropy may show a discrepancy between rheology measurements and compression tests.

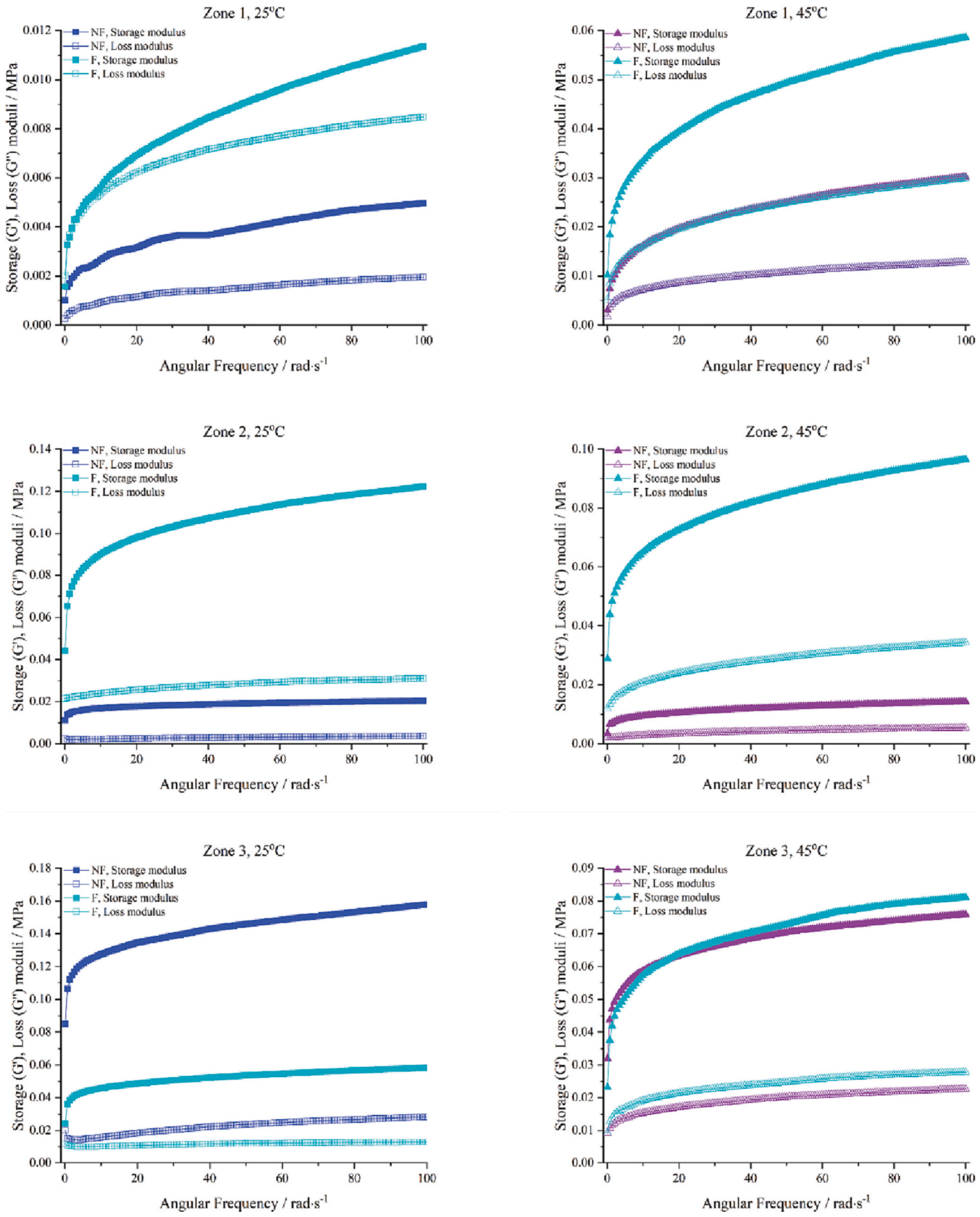

Fig. 7. Graphs of frequency sweeps of the different zones observed at non-frozen and frozen HPC hydrogels.

Table 2
Values of storage (G′) and loss (G″) modulus[a] of frequency sweep plots of non-frozen and frozen samples of Z1, Z2, and Z3.

Zone 1				
Temp./ °C	Not frozen		Frozen	
	Storage M. (G′)/ MPa	Loss M. (G″)/ MPa	Storage M. (G′)/ MPa	Loss M. (G″)/ MPa
25 °C	0.005	0.002	0.011	0.009
35 °C	0.026	0.012	0.032	0.016
45 °C	0.030	0.013	0.059	0.030
55 °C	0.027	0.012	0.095	0.047

Temp. (°C)	Not frozen		Frozen	
	Storage M. (G′)/ MPa	Loss M. (G″)/ MPa	Storage M. (G′)/ MPa	Loss M. (G″)/ MPa
Zone 2				
25 °C	0.020	0.004	0.122	0.031
35 °C	0.022	0.007	0.114	0.034
45 °C	0.014	0.005	0.097	0.034
55 °C	0.020	0.010	0.098	0.039
Zone 3				
25 °C	0.158	0.028	0.058	0.013
35 °C	0.234	0.061	0.049	0.014
45 °C	0.076	0.023	0.081	0.028
55 °C	0.027	0.012	0.095	0.047

[a] Highest recorded values are reported from each plot.

4. Conclusions

In summary, we have demonstrated the fabrication, in a straightforward manner, and freezing of HPC hydrogels with graded porosity by taking advantage of its thermo-responsive phase-separation behavior. SEM imaging revealed a reduction in pore size along the cross-section of the HPC hydrogel from the top (~220 μm) to the bottom layer (~3 μm). A tracer's dye test was conducted to monitor the fluid dispersion through the gradient HPC hydrogel column. The results showed the non-permeability of the column due to the top layer having a closed-pore structure. After freezing, however, the resulting gel showed high liquid permeability. The mechanical properties of graded HPC hydrogel layers were investigated through uniaxial compression testing and rheology. It was found that the layer exposed to temperatures at/above 42 °C compressed to approximately 80% without fracture and exhibited the predominant mechanical properties of toughness and softness, while the layer cross-linked at room temperature showed a fracture at about 49%. However, the same layer after freezing-thawing treatment maintained its structure and exhibited around 53% compression strain. Thus, besides introducing pore connectivity, freezing can also improve gel mechanical properties, in this case leading to a gel monolith with increasing compressive modulus from the top to the bottom of the monolith.

This work presents the first example of introducing a graded structure into a hydrogel by exploiting its intrinsic thermoresponsive properties, and demonstrates the feasibility of utilizing polymer LCST for structural control, which could be used in future work for other thermoresponsive polymers. Such a concept could be extended further to other stimuli-responsive materials properties, such as photo-responsiveness, whereby a graded stimulus could be used to create corresponding structural gradients. Here, the permeable graded structure of the HPC hydrogel was prepared by varying temperatures between the top and bottom layers of the monolith sample. Such graded structures can have an impact as filtration materials, tissue scaffolds, implants, or in applications taking advantage of their graded mechanical strength and elastic properties particularly as they can be easily strengthened via post-casting mineralization processes.

CRediT authorship contribution statement

Alexia Tialiou: Experimental work, Data curation, Validation, Investigation, Writing.

Zahraa H. Athab: Initial experimental work, Writing.

Jia Min Chin: Conceptualization, Supervision, Validation, Writing – Review & Editing, Funding acquisition.

Michael R. Reithofer: Conceptualization, Supervision, Validation, Writing – Review & Editing.

Robert T. Woodward: Supervision, Review & Editing.

Veronika Biegler: Experimental work, Data curation.

Bernhard Keppler: Supervision.

Ahmed F. Halbus: Writing.

Declaration of competing interest

The authors declare that they have no known competing financial interests or personal relationships that could have appeared to influence the work reported in this paper.

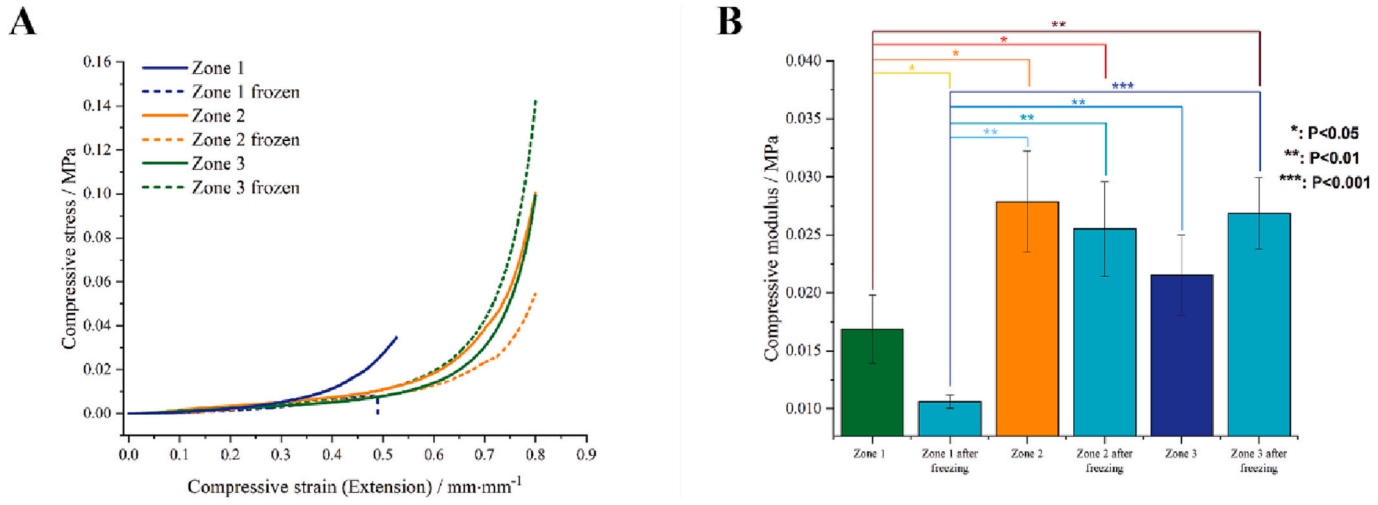

Fig. 8. (A) Compressive stress-strain curves of gHPC hydrogel layers before freezing and after freezing at −20 °C for three days and subsequent thawing; (B) Compressive modulus of the gHPC layers before and after freezing – 20 °C for three days and thawing. Each measurement was carried out five times, each time using a new sample. For these measurements, one way ANOVA was performed (*:P < 0.05, **P:<0.01, ***P:<0.001).

Data availability

Data will be made available on request.

Acknowledgments

We acknowledge support in supplying the infrastructure for SEM imaging by the Faculty Center for Nano Structure Research at the University of Vienna and S. Puchegger's contribution. We also acknowledge support from Q. Zhang with rheological measurements. A. T. thanks the University of Vienna for the financial support for her Ph.D. study. Z.H.A. thanks the Iraqi Government, the Higher Committee for Education Development of Iraq, and the University of Babylon, Iraq for the financial support for her Ph.D. study during the work on this project. J. C. also acknowledges support from the ERC CoG (101002176).

Appendix A. Supplementary data

Supplementary data to this article can be found online at https://doi.org/10.1016/j.carbpol.2023.120984.

References

Ahmed, A., Smith, J., & Zhang, H. (2011). Gradient porous materials by emulsion centrifugation. *Chemical Communications, 47*(42), 11754.
Annabi, N., Nichol, J. W., Zhong, X., Ji, C., Koshy, S., Khademhosseini, A., & Dehghani, F. (2010). Controlling the porosity and microarchitecture of hydrogels for tissue engineering. *Tissue Engineering Part B: Reviews, 16*(4), 371–383.
Asoh, T.-A., Matsusaki, M., Kaneko, T., & Akashi, M. (2008). Fabrication of temperature-responsive bending hydrogels with a nanostructured gradient. *Advanced Materials, 20*(11), 2080–2083.
Bencherif, S. A., Sands, R. W., Bhatta, D., Arany, P., Verbeke, C. S., Edwards, D. A., & Mooney, D. J. (2012). Injectable preformed scaffolds with shape-memory properties. *Proceedings of the National Academy of Sciences, 109*(48), 19590–19595.
Castillo, M., Moore, J. J., Schowengerdt, F. D., Ayers, R. A., Zhang, X., Umakoshi, M., & Guigne, J. Y. (2003). Effects of gravity on combustion synthesis of functionally graded biomaterials. *Advances in Space Research, 32*(2), 265–270.
Chabera, P., Boczkowska, A., Witek, A., & Oziębło, A. (2015). Fabrication and characterization of composite materials based on porous ceramic preform infiltrated by elastomer. *Bulletin of the Polish Academy of Sciences Technical Sciences, 63*(1), 193–199.
Einsiedl, F., & Maloszewski, P. (2005). Tracer tests in fractured rocks with a new fluorescent dye—pyrene-1,3,6,8-tetra sulphonic acid (PTS) / tests de traçage en roches fracturées avec un nouveau produit fluorescent—l'acide pyrène 1.3.6.8 tétra sulfonique (PTS). *Hydrological Sciences Journal, 50*(3).
Glassman, M. J., & Olsen, B. D. (2015). Arrested phase separation of elastin-like polypeptide solutions yields stiff, thermoresponsive gels. *Biomacromolecules, 16*(12), 3762–3773.
Grenier, J., Duval, H., Barou, F., Lv, P., David, B., & Letourneur, D. (2019). Mechanisms of pore formation in hydrogel scaffolds textured by freeze-drying. *Acta Biomaterialia, 94*, 195–203.
Gun'Ko, V. M., Savina, I. N., & Mikhalovsky, S. V. (2013). Cryogels: Morphological, structural and adsorption characterisation. *Advances in Colloid and Interface Science, 187–188*, 1–46.
Harsh, D. C., & Gehrke, S. H. (1991). Controlling the swelling characteristics of temperature-sensitive cellulose ether hydrogels. *Journal of Controlled Release, 17*(2), 175–185.
Kabra, B. G., Gehrke, S. H., & Spontak, R. J. (1998). Microporous, responsive hydroxypropyl cellulose gels. 1. Synthesis and microstructure. *Macromolecules, 31*(7), 2166–2173.
Klemm, D., Heublein, B., Fink, H.-P., & Bohn, A. (2005). Cellulose: Fascinating biopolymer and sustainable raw material. *Angewandte Chemie International Edition, 44*(22), 3358–3393.
Luo, R., Wu, J., Dinh, N.-D., & Chen, C.-H. (2015). Gradient porous elastic hydrogels with shape-memory property and anisotropic responses for programmable locomotion. *Advanced Functional Materials, 25*(47), 7272–7279.
Matricardi, P., Alhaique, F., & Coviello, T. (2016). *Polysaccharide hydrogels*. New York: Jenny Stanford Publishing.
Miao, X., & Sun, D. (2009). Graded/gradient porous biomaterials. *Materials, 3*(1), 26–47.
Mopoung, S., Sriprang, N., & Namahoot, J. (2014). Sintered filter materials with controlled porosity for water purification prepared from mixtures with optimal ratio of zeolite, bentonite, kaolinite, and charcoal. *Applied Clay Science, 88–89*, 123–128.
Myrick, J. M., Vendra, V. K., Le, N.-T., Sexton, F. A., & Krishnan, S. (2019). Controlled release of glucose from orally delivered temperature- and pH-responsive polysaccharide microparticle dispersions. *Industrial & Engineering Chemistry Research, 58*(46), 21056–21069.
Nakamura, C., Yamamoto, T., Manabe, K., Nakamura, T., Einaga, Y., & Shiratori, S. (2019). Thermoresponsive, freezing-resistant smart windows with adjustable transition temperature made from hydroxypropyl cellulose and glycerol. *Industrial & Engineering Chemistry Research, 58*(16), 6424–6428.
Otoni, C. G., Lorevice, M. V., Moura, M. R. D., & Mattoso, L. H. C. (2018). On the effects of hydroxyl substitution degree and molecular weight on mechanical and water barrier properties of hydroxypropyl methylcellulose films. *Carbohydrate Polymers, 185*, 105–111.
Plieva, F. M., Galaev, I. Y., Noppe, W., & Mattiasson, B. (2008). Cryogel applications in microbiology. *Trends in Microbiology, 16*(11), 543–551.
Rahimian, K., Wen, Y., & Oh, J. K. (2015). Redox-responsive cellulose-based thermoresponsive grafted copolymers and in-situ disulfide crosslinked nanogels. *Polymer, 72*, 387–394.
Richardson, S., Andersson, T., Brinkmalm, G., & Wittgren, B. (2003). Analytical approaches to improved characterization of substitution in hydroxypropyl cellulose. *Analytical Chemistry, 75*(22), 6077–6083.
Souzandeh, H., Scudiero, L., Wang, Y., & Zhong, W.-H. (2017). A disposable multi-functional air filter: Paper towel/protein nanofibers with gradient porous structures for capturing pollutants of broad species and sizes. *ACS Sustainable Chemistry & Engineering, 5*(7), 6209–6217.
Suk, M.-J., Choi, S.-I., Kim, J.-S., Kim, Y. D., & Kwon, Y.-S. (2003). Fabrication of a porous material with a porosity gradient by a pulsed electric current sintering process. *Metals and Materials International, 9*(6), 599–603.
Sultan, S., & Mathew, A. P. (2018). 3D printed scaffolds with gradient porosity based on a cellulose nanocrystal hydrogel. *Nanoscale, 10*(9), 4421–4431.
Taylor, M. J., Tomlins, P., & Sahota, T. S. (2017). Thermoresponsive gels. *Gels, 3*(1).
Thieme, M., Wieters, K. P., Bergner, F., Scharnweber, D., Worch, H., Ndop, J., & Grill, W. (2001). Titanium powder sintering for preparation of aporous functionally graded material destined fororthopaedic implants. *Journal of Materials Science: Materials in Medicine, 12*(3), 225–231.
Vida-Simiti, I., Jumate, N., Thalmaier, G., Sechel, N., & Moldovan, V. (2012). Study of gradual porous metallic membranes obtained by powder sedimentation. *Journal of Porous Materials, 19*(1), 21–27.
Wang, C., Chen, X., Wang, B., Huang, M., Wang, B., Jiang, Y., & Ruoff, R. S. (2018). Freeze-casting produces a graphene oxide aerogel with a radial and centrosymmetric structure. *ACS Nano, 12*(6), 5816–5825.
Wang, K., Yin, R., Lu, Y., Qiao, H., Zhu, Q., He, J., & Zhang, W. (2021). Soft-hard hybrid covalent-network polymer sponges with super resilience, recoverable energy dissipation and fatigue resistance under large deformation. *Materials Science and Engineering: C, 126*, Article 112185.
Wegst, U. G. K., Bai, H., Saiz, E., Tomsia, A. P., & Ritchie, R. O. (2015). Bioinspired structural materials. *Nature Materials, 14*(1), 23–36.
Weißenborn, E., & Braunschweig, B. (2019). Hydsroxypropyl cellulose as a green polymer for thermo-responsive aqueous foams. *Soft Matter, 15*(13), 2876–2883.
Werbowyj, R. S., & Gray, D. G. (1980). Ordered phase formation in concentrated hydroxypropylcellulose solutions. *Macromolecules, 13*(1), 69–73.
Werner, J., Linner-Krčmar, B., Friess, W., & Greil, P. (2002). Mechanical properties and in vitro cell compatibility of hydroxyapatite ceramics with graded pore structure. *Biomaterials, 23*(21), 4285–4294.
Zuo, K.-H., Zhang, Y., Jiang, D., & Zeng, Y.-P. (2011). Gradient porous hydroxyapatite ceramics fabricated by freeze casting method. *IOP Conference Series: Materials Science and Engineering, 18*(18), Article 182011.